05,07

Microstructure, crystal structure, dielectric and piezoelectric properties of solid solutions $SrBi_{2-x}Nd_xNb_2O_9$ ($x = 0.0, 0.1, 0.2, 0.3$)

© S.V. Zubkov[1], I.A. Parinov[2], A.V. Nazarenko[3], Yu.V. Prus[4,5]

[1] Southern Federal University, Research Institute of Physics, Rostov-on-Don, Russia
[2] I.I. Vorovich Institute of Mathematics, Mechanics and Computer Science, Southern Federal University, Rostov-on-Don, Russia
[3] Southern Scientific Center, Russian Academy of Sciences, Rostov-on-Don, Russia
[4] All-Russian Scientific Research Institute for Civil Defence and Emergencies of the EMERCOM of Russia, Moscow, Russia
[5] Academy of the State Fire Service of the EMERCOM of Russia, St. Petersburg, Russia

E-mail: svzubkov61@mail.ru

Received July 8, 2025
Revised July 28, 2025
Accepted July 31, 2025

A new series of solid solutions of the Aurivillius-Smolensky phase family $SrBi_{2-x}Nd_xNb_2O_9$ ($x = 0.0$, 0.1, 0.2, 0.3) was synthesized by the high-temperature solid-phase reaction method. X-ray diffraction analysis showed that all the synthesized compounds are single-phase and have the structure of the Aurivillius-Smolensky phase family (ASF) with parameters close to the orthorhombic unit cell corresponding to the space group $A2_1am$. For the synthesized compound, the temperature dependences of the relative permittivity $\varepsilon/\varepsilon_0$ and the loss tangent $\mathrm{tg}\,\sigma$ at different frequencies, as well as the piezoelectric modulus d_{33} were measured; the microstructure and hysteresis loops were investigated.

Keywords: Aurivillius-Smolensky phases, $SrBi_{2-x}Nd_xNb_2O_9$, Curie temperature T_C, microstructure, permittivity $\varepsilon/\varepsilon_0$.

DOI: 10.61011/PSS.2025.08.62262.179-25

1. Introduction

When studying the system $Bi_2O_3-TiO_2$ in 1949, V. Aurivillius established that the $Bi_4Ti_3O_{12}$ oxide with a perovskite-type structure was formed [1]. Ten years later, the G. Smolenskii's team [2] discovered ferroelectric properties in $Bi_2PbNb_2O_9$ that belongs to this compound family, which was followed by an intense stage of investigation of these compounds. In 1961 and 1962, E.S. Subbarao produced about ten new compounds and almost all of them were ferroelectric [3,4]. In this regard, these compounds can be rightfully called Aurivillius–Smolensky phases (ASP) [5].

As of now, hundreds of the ASPes are synthesized. They form a large family of bismuth-containing perovskite-type layered compounds, whose chemical composition is described by the general formula $Bi_2A_{m-1}B_mO_{3m+3}$. The ASP crystal structure includes alternating layers $[Bi_2O_2]^{2+}$ that are separated by m perovskite-like layers $[A_{m-1}B_mO_{3m+1}]^{2-}$, where A sites are occupied by large-radius ions: Na^+ [6], K^+ [7], Ca^{2+} [8], Sr^{2+} [9], Ba^{2+} [10], Pb^{2+} [11], Y^{3+} [12,13], Bi^{3+}, Ln^{3+} (La [14], Nd [15], Sm [16], Gd [17], Ce [18], Tb [19], Dy [20], Ho [21], Er [22], Eu [23]) and Ac, Th, Pr (actinides), which demonstrate a dodecahedral coordination. B-sites inside the oxygen octahedrons are occupied by highly-charged ($\geq 3+$) low-radius cations: Fe, Cr, Mn, Co, [24–26] as well as Cu^{2+} [27], Mg^{2+} [28], Ti^{4+}, W^{6+} [29], Nb^{5+} [30], Ta^{5+} [31].

The value of m is determined by the number of the perovskite layers $[A_{m-1}B_mO_{3m+1}]^{2-}$ arranged between fluorite-like layers $[Bi_2O_2]^{2+}$ along a pseudo-tetragonal axis c [32] and can be an integer or semi-integer [33] number within the range $m = 1-5$. Replacements of atoms in the sites A and B significantly affect electric properties of the ASP. There are large changes of permittivity and electrical conductivity; besides, the Curie temperature can also T_C vary widely. Thus, the study of the cation-substituted ASP compounds is of great importance in the development of materials for various technical purposes.

A microstructure and electric properties of the ASP compound family $SrBi_2Nb_20_9$ (SBN) are studied due to a report on a high piezoelectric constant $d_{33} \leq 20$ pC/N, low dielectric losses [34–38] and its excellent no-fatigue properties [39–44], thereby making this compound a base for creating new piezoelectric materials.

Replacement of Sr in the sites with Ca ions in the SBM ceramic resulted in crease of T_C, which is important for high-temperature resonant cavity applications [45,46]. But, replacement of Bi^{3+} in the Bi_2O_2 layers with some rare-earth ions, such as La^{3+} or Pr^{3+}, results in shifting T_C

towards the lower temperatures [47–49]. It was found that a behavior of the neodymium-doped SBN ceramic resulted in a transition from the common ferroelectric into a relaxor-type ferroelectric due to incorporation of Nd^{3+} ions into the Bi_2O_2 layers [50,51]. It was reported in the study [52] that the $SrBi_{1.8}Pr_{0.2}Nb_2O_9$ ceramic demonstrated a relaxor behavior of frequency dispersion. Replacement of the Bi^{3+} ions with Nd^{3+} resulted in shifting the Curie temperature T_C towards the lower temperatures, reduction of residual polarization and reduction of a coercive field.

The present study has investigated the influence of replacement of the Bi^{3+} ions with the Nd^{3+} ions on the crystal microstructure, dielectric, ferroelectric and piezoelectric properties of the synthesized ASP compounds $SrBi_{2-x}Nd_xNb_2O_9$ ($x = 0.0,\ 0.1,\ 0.2,\ 0.3$).

The present study continues a series of studies on investigating the crystal structure, the microstructure, the Curie temperature T_C, the dielectric and ferroelectric properties of the various compounds of the ASP family when doping with the neodymium ions [53–56].

2. Experiment

The polycrystalline ASP series $SrBi_{2-x}Nd_xNb_2O_9$ ($x = 0.0,\ 0.1,\ 0.2,\ 0.3$) was synthesized by a solid-state reaction of the respective oxides Bi_2O_3, $SrCO_3$, Nd_2O_3, Nb_2O_5. All original compounds were of analytic grade. After weighing in a stoichiometric composition and thorough fining of the initial oxides with addition of ethanol, the pressed samples were ignited at the temperature 860−870 °C for 4h. The samples were calcinated in a muffle furnace in air. The sample was then crushed, repeatedly fined and pressed into pills of a diameter of 9 mm and a thickness 1.0−1.5 mm, with subsequent final synthesis at the temperature of 1140 °C (2 h).

The X-ray image was recorded at a diffractometer Rigaku Ultima IV with a Cu X-ray tube. Radiation Cu Kα_1, α_2 was picked up out of the general spectrum by means of a Ni filter. The X-ray image was measured within an angle range of 2θ from 10° to 60° with a scanning step of 0.02° and exposure (intensity recording time) of 4 s per dot. Analysis of the X-ray image profile, determination of line positions, their indexing (hkl) and refinement of lattice cell parameters was carried out using the PCW software 2.4 [57].

In order to measure the permittivity and electric conductivity, electrodes were applied onto flat surfaces of the studied samples using Ag paste annealed at the temperature of 720 °C (20 min.). The temperature and frequency characteristics of the dielectric characteristics were measured using an E7-20 LCR meter in the frequency range from 100 kHz to 1 MHz and in the temperature range from the room temperature to 500 °C.

The piezoelectric constant d_{33} was measured by polarizing the sample in an oil bath at 150 °C under voltage 45−65 kV/cm for 30 min.

Hysteresis loops $P-E$ were studied using the Sawyer−Tower circuit of a bench for studying piezoelectric materials in strong electric fields „Petlya“ [58]. The measurement were performed at the room temperature with the maximum voltage ~ 5 kV by immersing the sample into oil. The values of the piezoelectric constant of the studied compounds were found from a relationship with the known value of the piezoelectric constant of a reference X-cut quartz sample.

Images of the microstructure of the surfaces were obtained by means of a scanning electron microscope Carl Zeiss EVO 40 (Germany) at the Collective Use Center of the Southern Scientific Center of the Russian Academy of Sciences. The study was carried out at transverse cleavages of the produced ceramic without preliminary mechanical processing. An additional conducting layer was neither applied. The images are obtained in a mode of high accelerating voltage (EHT = 20 kV), and the probe current was $I_{probe} = 25$ pA, while the operating distance was $WD = 7.5-8$ mm.

3. Results and their discussion

Powder X-ray diffraction patterns of all the studied solid solutions $SrBi_{2-x}Nd_xNb_2O_9$ ($x = 0.0,\ 0.1,\ 0.2,\ 0.3$) correspond to the single-phase ASPes with $m = 2$ and have not additional reflections. These compounds are isostructural to the known perovskite-like oxide of the SBN ASP. All the peaks are indexed based on orthorhombic cells related to a space group $A2_1am$, which corresponds to the JCPDS file of №. 49-0617 (№. 36 in the PCW 2.4 software). Figure 1, *a* shows the experimental powder X-ray diffraction pattern of the studied compounds $SrBi_{2-x}Nd_xNb_2O_9$ ($x = 0.0,\ 0.1,\ 0.2,\ 0.3$). The peak (115) in the X-ray diffraction pattern of Figure 1, *a* shows the highest intensity in the plane $(11(2m+1))$. This typical diffraction peak corresponds to a layered structure of SBN [59].

It is clear that a degree of orientation of the $00l$ ceramic remains constant and does not depend on the concentration of Nd^{3+}, which is typical when sintering for a short ($t < 25$ h) time. It is clear in Figure 1, *b*) that the peak (115) is shifted towards a larger angle when increasing x from 0.0 to 0.3.

3.1. Microstructure

The microstructure of the studied portions of the ceramic $SrBi_{2-x}Nd_xNb_2O_9$ ($x = 0.0,\ 0.1,\ 0.2,\ 0.3$) is identical at the concentrations of x up to 0.2 (Figure 2); there are chaotically densely-packed crystallites, whose sizes vary from $\sim 0.8\,\mu$m to $\sim 5.0\,\mu$m. Generally, the grains have a homogeneous internal structure, but in some areas, where they are inclined to a cleavage plane, there are heterogeneities that are a stack of layers of a submicron thickness (Figure 2, the selected areas and arrows). Despite the fact that when $x = 0.1$ the size distribution is slightly wider and less homogeneous than

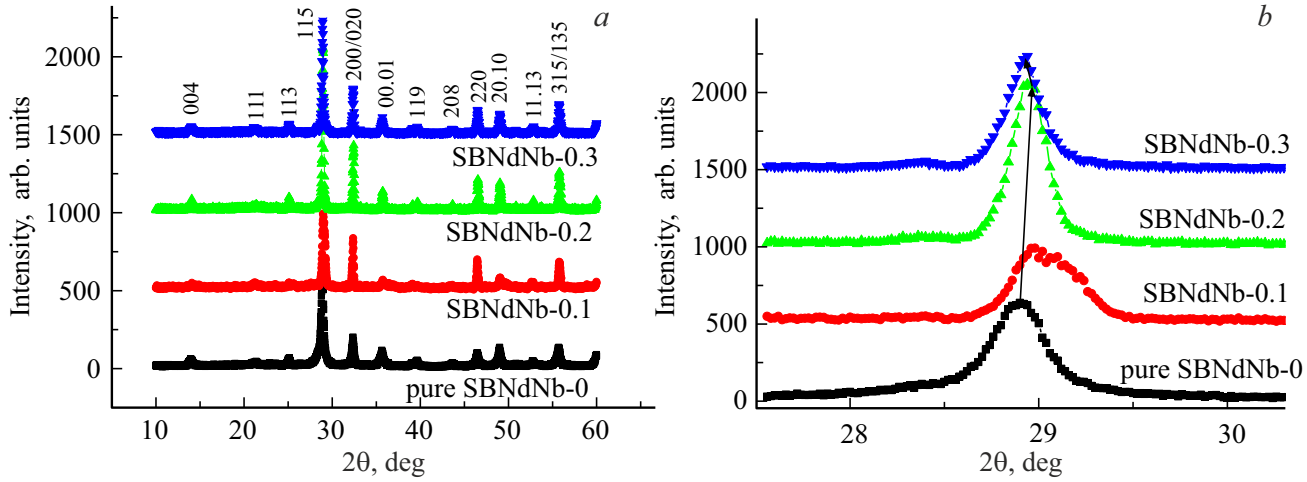

Figure 1. X-ray diffraction patterns of the ceramic $SrBi_{2-x}Nd_xNb_2O_9$ ($x = 0.0, 0.1, 0.2, 0.3$) within the range of 2θ, $10°-60°$.

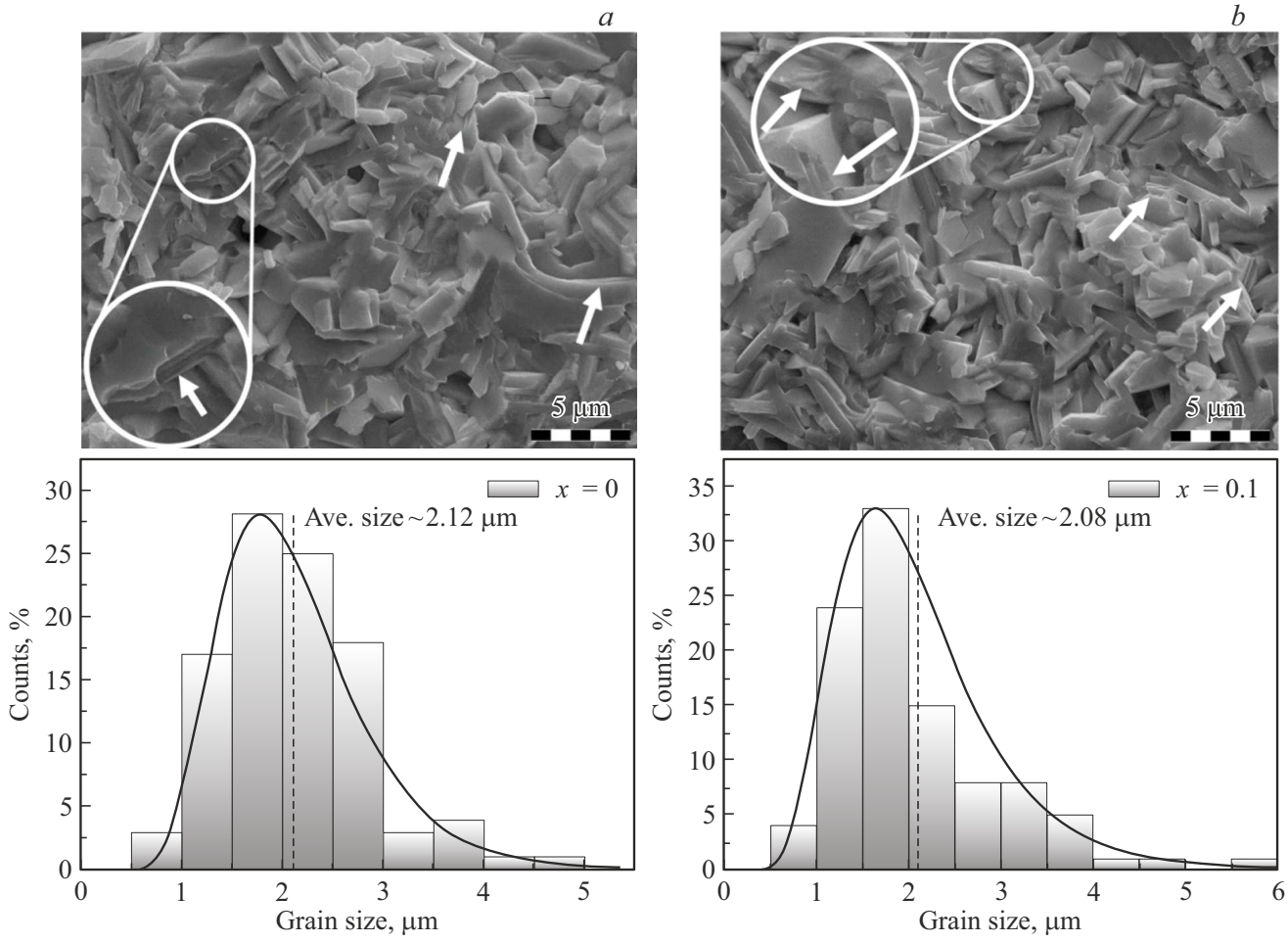

Figure 2. Microstructures and distribution of grain sizes when $x = 0.0$ (a) and $x = 0.1$ (b).

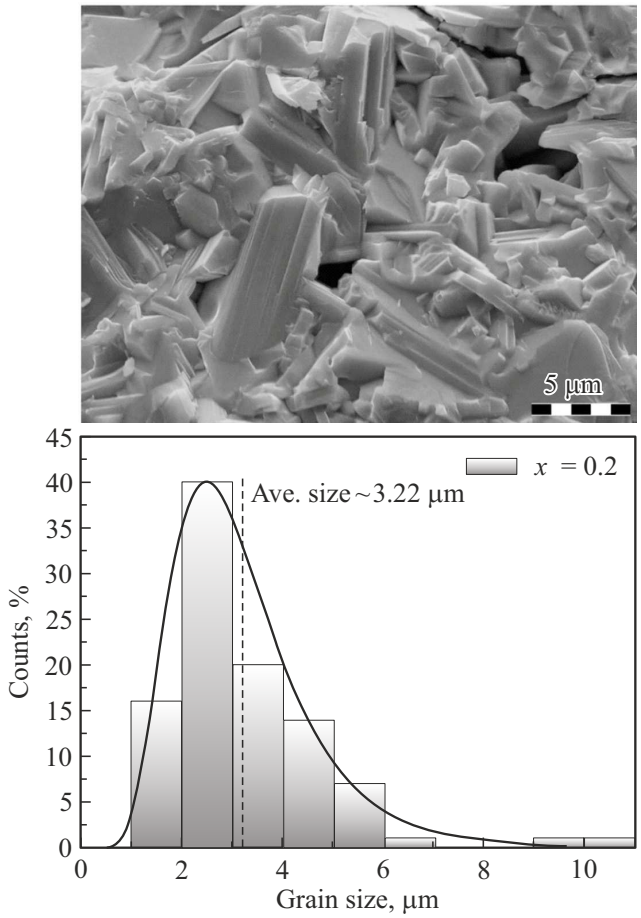

Figure 3. Microstructure and distribution of grain sizes when $x = 0.2$.

in the case when $x = 0.0$, their forms are approximated by almost identical lognormal curves and 90% of the grain sizes stay within the range from $1.0\,\mu$m to $3.0-3.5\,\mu$m, with almost the same average size value of about $2.1\,\mu$m.

When $x = 0.2$, the ceramic structure is less dense and exhibits cracks and pores of a partially technological and diffusion nature (Figure 2). The grains also merge chaotically, while their internal structure becomes generally inhomogeneous (the layered structure can be seen almost everywhere). At the same time, the grains look much larger and thicker. Their maximum size can be up to $\sim 11\,\mu$m, while an average growth is about 34% in contrast to the grains in the samples with the concentrations $x = 0.0-0.1$.

Analysis of size distribution of the crystallites when$x = 0.2$ also shows a lognormal behavior, which is more uniform and has a „heavier tail" than in case when $x = 0.0-0.1$. Here, 90% of the sizes are in a wider range $1-5\,\mu$m. The average grain size is about $3.2\,\mu$m.

The microstructure analysis has shown that the ceramics were cleaved predominantly along the grains, while the ceramic itself had a high density. The grains are mainly flat and irregularly-shaped and have quite well-defined boundaries. It indicates an anisotropic of crystallites, which is typical for the ASP family. The localized pores can have both the technological as well as diffusion nature, which seems to change with an increase of the concentration. With the increase of the concentration, the average grain size increases from $\sim 2.1\,\mu$m to $\sim 3.2\,\mu$m, too, which can affect physical-mechanical properties of the materials.

3.2. Crystal lattice

The X-ray diffraction data were used to determine parameters of the lattice cell (the lattice constants a_0, b_0, c_0 and the volume V), which are listed in Table 1.

Table 1 also shows parameters of orthorhombic δb_0 and tetragonal $\delta c'$ deformation; the average tetragonal period a_t, the average thickness of one perovskite-like layer c'; $c' = 3c_0/(8 + 6\text{m})$, $a_t = (a_0 + b_0)/(2\sqrt{2})$ — the average value of the tetragonal period; a_0, b_0, c_0 — the lattice periods; $\delta c' = (c' - a_t)/a_t$ — deviation of the cell from the cubic form, i.e. elongation or contraction of the cubic form; $\delta b_0 = (b_0 - a_0)/a_0$ — orthorhombic deformation [60,61]. The obtained parameters of the lattice cell of the studied sample $SrBi_2Nb_2O_9$: $a = 5.55$ Å, $b = 5.48$ Å, $c = 25.261$ Å [62].

A tolerance factor t was introduced by V.M. Goldschmidt [63] as a geometric criterion that determines a degree of stability and distortion of the crystal structure:

$$t = (R_A + R_O) / \left[\sqrt{2}(R_B + R_O)\right], \qquad (1)$$

where R_A and R_B — the cation radii in the sites A and B, respectively; R_O — the ion radius of oxygen. The values of the tolerance factor t for the studied sample are given in Table 2. The tolerance factor was calculated in the present study taking into account a table of the R.D. Shannon ionic radii [64] for the respective coordination numbers (CN) (O^{2-} (CN = 6), $R_O^{2-} = 1.40$ Å; Nb^{5+} (CN = 12), $R_{Nb^{5+}} = 0.64$ Å. Shannon did not provide the ionic radius of Bi^{3+} for coordination with CN = 12. Therefore, its value was determined from the ionic radius with CN = 8 ($R_{Bi^{3+}} = 1.17$ Å), which is multiplied by the approximation coefficient of 1.179, whereas for Bi^{3+} (CN = 12) $R_{Bi^{3+}} = 1.38$ Å.

3.3. Dielectric properties

Figure 4 shows the dependences of relative permittivity $\varepsilon/\varepsilon_0$ and the dielectric loss angle tangent $\operatorname{tg}\delta$ on the temperature for ASP $SrBi_{2-x}Nd_xNb_2O_9$ ($x = 0.0$, 0.1, 0.2, 0.3) at the frequency values from 100 kHz to 1 MHz for the ceramics sintered at the temperatures of 1140 °C.

The permittivity maximum that corresponds to the „ferroelectric–paraelectric" phase transition (CT) is clearly observed for a series of the solid solutions $SrBi_{2-x}Nd_xNb_2O_9$ ($x = 0.0$, 0.1) at the frequencies from 100 kHz to 1 MHz. It is also possible for this series to observe a correspondence of the minimum of $\operatorname{tg}\delta$ within the area of the Curie temperature T_C. A smeared maximum of $\varepsilon/\varepsilon_0(T)$ is observed for the series $SrBi_{2-x}Nd_xNb_2O_9$

Table 1. Parameters of the lattice cell a_0, b_0, c_0, V, a_t — the parameter of the tetragonal period, c' — the height of the octahedron along the axis c, $\delta c'$ — deviation from the rhombic form, δb_0 — rhombic distortion

Compounds	a_0, Å	b_0, Å	c_0, Å	V, Å^3	c', Å	a_t, %	$\delta c'$, %	δb_0, %
$SrBi_2Nb_2O_9$	551	5.5	25.16	762.474	3.774	3.893	−3.08	−0.20
$SrBi_{1,9}Nd_{0,1}Nb_2O_9$	5.539	5.518	25.161	769.025	3.7742	3.909	−3.40	−0.37
$SrBi_{1,8}Nd_{0,2}Nb_2O_9$	5.542	5.515	25.355	774.935	3.80	3.909	−2.80	−0.48
$SrBi_{1,7}Nd_{0,3}Nb_2O_9$	5.538	5.512	25.308	772.538	3.796	3.906	−2.80	−0.47

Table 2. Tolerance t-factor, the Curie temperatureT_C, relative permittivity $\varepsilon/\varepsilon_0$ and loss tangent $\operatorname{tg}\delta$, which are measured at the frequency of 100 kHz, piezoelectric constant d_{33}.

№	Compounds	t-factor	T, °C	$\varepsilon/\varepsilon_0$	$\operatorname{tg}\delta$	d_{33}, pC/H
1	$SrBi_2Nb_2O_9$	0.971	421	646	0.4	7.6
2	$SrBi_{1.9}Nd_{0.1}Nb_2O_9$	0.969	375	386	0.15	7.0
3	$SrBi_{1.8}Nd_{0.2}Nb_2O_9$	0.968	318	275	0.022	7.8
4	$SrBi_{1.7}Nd_{0.3}Nb_2O_9$	0.966	235	204	0.012	5.1

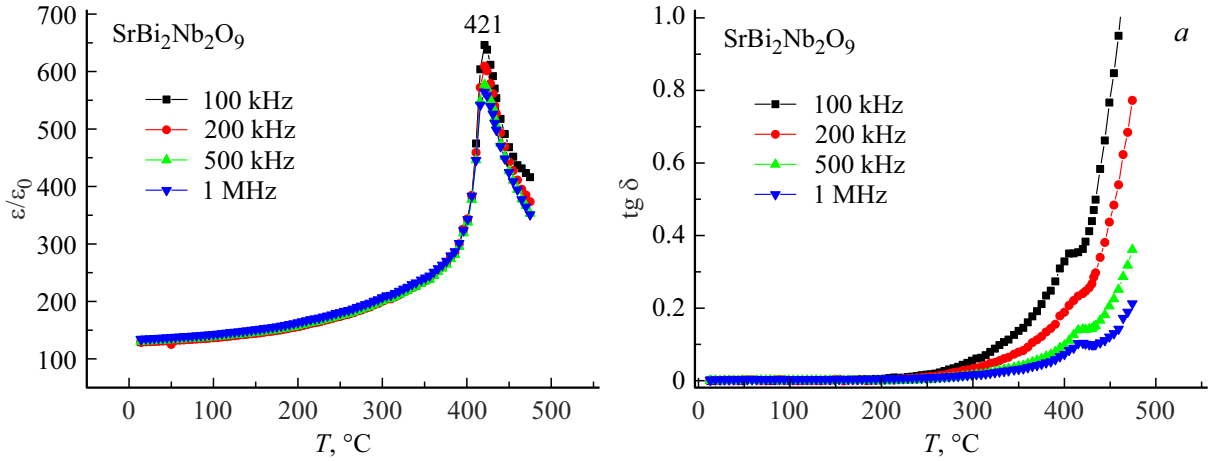

Figure 4. Temperature dependences of relative permittivity $\varepsilon/\varepsilon_0(T)$ (a, b) and $\operatorname{tg}\delta$ for $SrBi_{2-x}Nd{-}xNb_2O_9$ $(x = 0.0, 0.1, 0.2, 0.3)$.

$(x = 0.2, 0.3)$, wherein a temperature of its maximum can be related to the phase transition temperature T_C. For $\operatorname{tg}\delta$, $SrBi_{2-x}Nd_xNb_2O_9$ does not exhibit the usual dependence of the Curie temperature T_C and the minimum of the value of $\operatorname{tg}\delta$ within the interval $x = 0.2{-}0.3$ (see Figure 4). Besides, there is also a shift of the minimum of $\operatorname{tg}\delta$ towards the higher values within the interval $x = 0.0{-}0.3$ from the phase transition temperature. It can be a more explicit feature of the relaxor properties of $SrBi_{2-x}Nd_xNb_2O_9$ $(x = 0.2, 0.3)$ as compared to a shift of $\varepsilon/\varepsilon_0(T)$ towards the higher values of the temperature with increase of the frequency (Figure 4, a). The relaxor properties of $SrBi_{2-x}Nd_xNb_2O_9$ within the interval $x = 0.2{-}0.3$ are attributed to the fact that the neodymium ions replace the bismuth ions not in the perovskite-like layer, but in the fluorite-like bismuth-oxygen $(Bi_2O_2)^{2+}$ layers.

With increase of the concentrations of the Nd^{3+} ions in the series of the synthesized compounds $SrBi_{2-x}Nd_xNb_2O_9$ $(x = 0.0, 0.1, 0.2, 0.3)$, there is reduction of the value of dielectric loss angle tangent $\operatorname{tg}\delta$ in almost 30 times (see Table 2) for $SrBi_{2-x}Nd_xNb_2O_9$ $(x = 0.3)$ as compared to the undoped SBN. Doping of the composition $SrBi_{2-x}Nd_xNb_2O_9$ $(x = 0.0, 0.1, 0.2, 0.3)$ with the Nd^{3+} ions results in a decrease of the dielectric loss angle tangent, thereby indicating reduction of the concentration of oxygen vacancies.

Figure 5 shows variation of the phase transition temperature T_C with increase of the concentration of $Nd^{3+}(x)$.

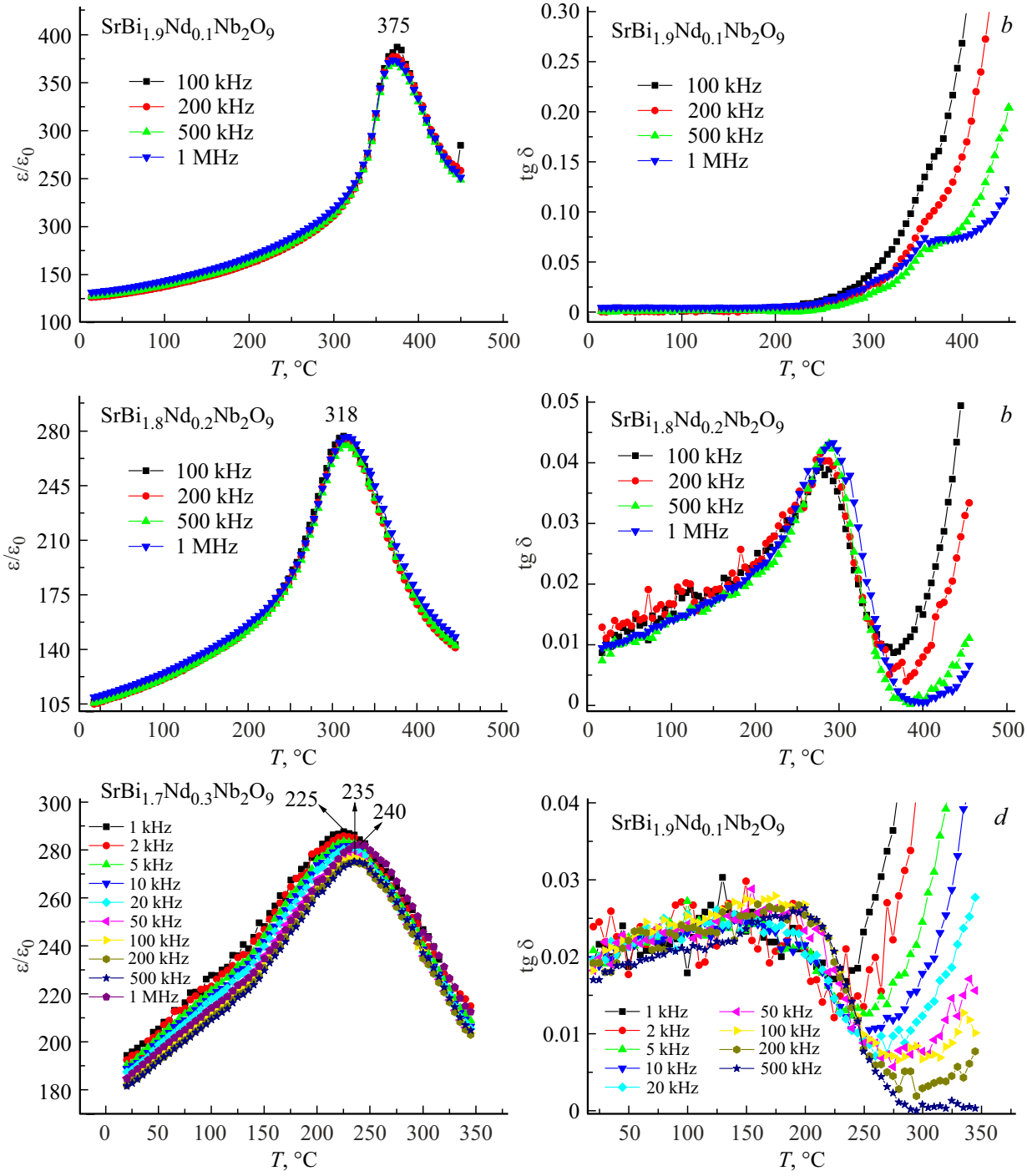

Figure 4 (*continued*).

The Curie temperature T_C decreases almost linearly with increase of the Nd dopant. A possible reason for this can be reduction of distortion of the NbO_6 octahedron for the ceramic $SrBi_{2-x}Nd_xNb_2O_9$ ($x = 0.0, 0.1, 0.2, 0.3$). The Bi^{3+} ion in the perovskite-like layer has one unshared pair of $6s^2$ electrons [65]. Besides, some studies have indicated that for ASP the fluorite-like Bi_2O_2 layers and the perovskite-like layers are under tensile and compressive stress [66,67] and, consequently, when replacing with the smaller-radius ion, the perovskite-like layers will experience smaller stress forces, thereby resulting in reduction of distortion of the oxygen octahedron.

Besides, the unshared pairs of electrons have a tendency of occupying more space than electrons of a binding pair in accordance with the valence shell electron pair repulsion theory. Thus, the degree of distortion of the

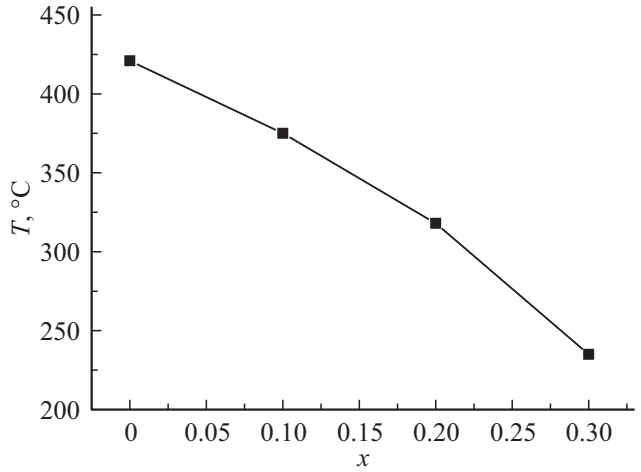

Figure 5. Dependence of the Curie temperature T_C on the concentration of Nd^{3+}.

NbO_6 octahedrons will decrease when Bi^{3+} are replaced with Nd^{3+} that have not unshared pairs of electrons.

It can explain reduction of the phase transition temperature with simultaneous reduction of the volume of the crystal cell V, Å^3 (Table 1).

3.4. Ferroelectric properties

Figure 6 shows the dependence P(E) for the series of the compounds $SrBi_{2-x}Nd_xNb_2O_9$ ($x = 0.0$, 0.1, 0.2, 0.3). The obtained hysteresis loops $P-E$ are not saturated and have an elongated shape. As can be seen, with partial replacement of Bi with Nd, residual polarizability P_r and the coercive force E_f practically did not change for $SrBi_{2-x}Nd_xNb_2O_9 - (0.0,\ 0.1,\ 0.2)$ as compared to SBN. For $SrBi_{2-x}Nd_xNb_2O_9$ ($x = 0.3$) residual polarizability P_r has increased in 2.5 time as compared to SBN.

3.5. Activation energy

The activation energy E_a was determined from the Arrhenius equation:

$$\sigma = (A/T)\exp\left[-E_a/(kT)\right] \tag{2}$$

where σ — electrical conductivity, k — the Boltzmann constant, A — the constant, E_a — the activation energy. The typical dependence of $\ln\sigma$ (σ-conductivity) on $10^4/T$ (at the frequency of 100 kHz), which has been used to determine the activation energy E_a, is shown in Figure 7 for ASP $SrBi_2Nb_2O_9$. The compounds $SrBi_{2-x}Nd_xNb_2O_9$

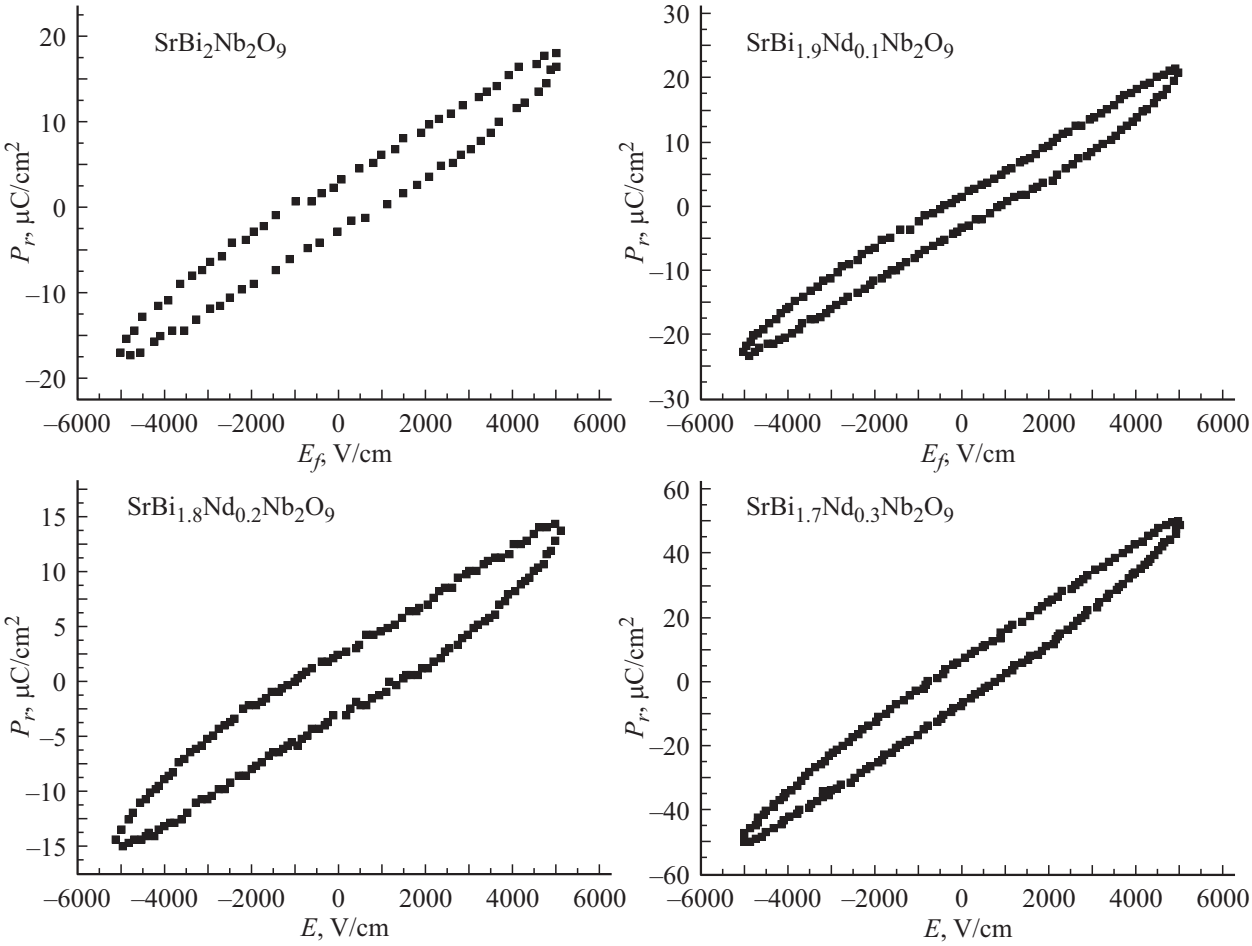

Figure 6. Hysteresis loops $P-E$ for the samples $SrBi_{2-x}Nd_xNb_2O_9$ ($x = 0.0$, 0.1, 0.2, 0.3).

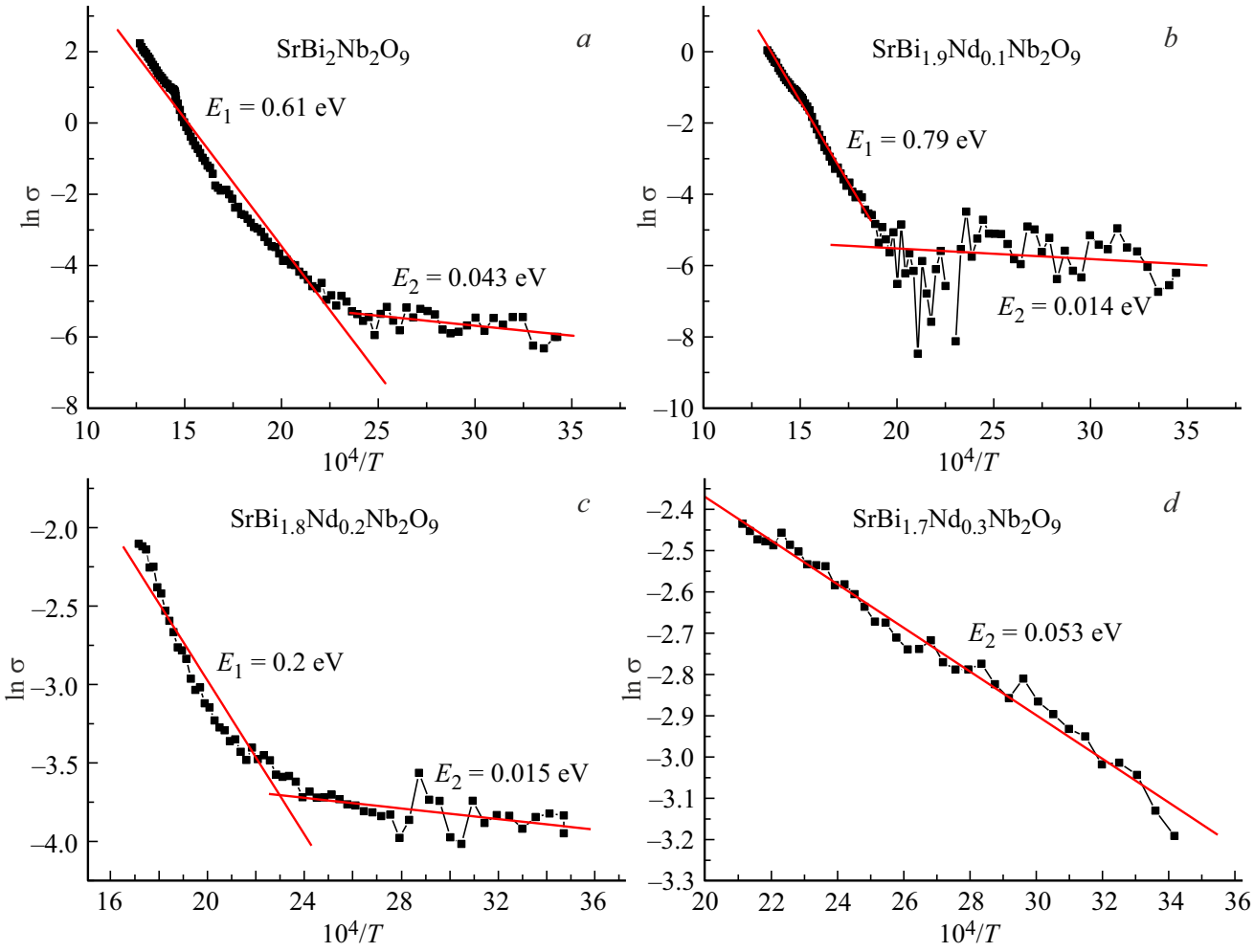

Figure 7. Dependence of $\ln\sigma$ on $10^4/T$ for $SrBi_{2-x}Nd_xNb_2O_9$ ($x = 0.0$, 0.1, 0.2, 0.3) at the frequency of 100 kHz.

($x = 0.0$, 0.1) have two temperature ranges in which the activation energy E_a differs significantly in a value. Within the low temperatures, electric conductivity is predominantly determined by impurity defects with very low activation energies of about one hundredth of an electronvolt. The intrinsic conductivity activation energy is $E_1 \sim 0.6-0.8$ eV. For the compounds $SrBi_{2-x}Nd_xNb_2O_9$ ($x = 0.2$, 0.3) of Figure 7, *b, c* such activation values do not exist, since the phase transition temperatures for $SrBi_{2-x}Nd_xNb_2O_9$ ($x = 0.2$, 0.3) are within a range of impurity conductivity temperatures (see Figure 5).

4. Conclusions

The present study has investigated electrophysical properties of the perovskite-like oxides of ASP for the solid solutions $SrBi_{2-x}Nd_xNb_2O_9$ ($x = 0.0$, 0.1, 0.2, 0.3).

The ceramic was made using the traditional method of solid-phase reaction. The X-ray diffraction patterns are indexed as orthorhombic $A2_1am$ for all the ASP solid solutions.

Doping with Nd^{3+} for the composition $SrBi_{2-x}Nd_xNb_2O_9$ ($x = 0.2$, 0.3) reduced the dielectric loss angle tangent in 30 times as compared to the undoped SBN.

The piezoelectric constant of the compound $SrBi_{2-x}Nd_xNb_2O_9$ ($x = 0.2$) is higher than for SBN, which is related to reduction of the oxygen vacancies.

The minimum Curie temperature $T_C = 235\,^\circ$C for the synthesized series was obtained for the compound $SrBi_{2-x}Nd_xNb_2O_9$ ($x = 0.3$).

Doping with Nd^{3+} reduced the Curie temperature T_C with increase of x. With increase of the concentration of Nd^{3+}, the relaxor properties of $SrBi_{2-x}Nd_xNb_2O_9$ ($x = 0.0$, 0.1, 0.2, 0.3) increased.

For the synthesized series of the compounds $SrBi_{2-x}Nd_xNb_2O_9$ ($x = 0.0$, 0.1, 0.2), residual polarizability P_r and the coercive force E_f remained almost unchanged. At the same time, for the compound $SrBi_{2-x}Nd_xNb_2O_9$ ($x = 0.3$) residual polarizability P_r increased almost in 2.5 times as compared to the undoped SBN compound with the almost unchanged coercive force E_f.

Acknowledgments

The microstructure was analyzed using the equipment of the Collective Use Center of the Southern Scientific Center of the Russian Academy of Sciences (No. 501994) under state assignment of the Southern Scientific Center of the Russian Academy of Sciences (No. FMRE-2025-0051).

Funding

The Institute of Analytical Instrumentation would like to thank for financial support as part of the scientific project No. FENW-2023-0012 under State research assignment.

Conflict of interest

The authors declare that they have no conflict of interest.

References

[1] B. Aurivillius. Arkiv. Kemi. **1**, *54*, 463–80 (1949).
[2] G.A. Smolensky, V.A. Isupov, A.I. Agranovskaya. Soviet Physics Solid State, **3**, 651–655 (1961).
[3] E.C. Subbarao. J. Am. Ceram. Soc. **45**, 166–169 (1962).
[4] E.C. Subbarao. J. Chem. Phys. **34**, 695–696 (1961).
[5] I.A. Parinov, S.V. Zubkov. J. Adv. Dielectr. **13**, 2340007 (2023).
[6] C. Long, C. Qi, W. Yun, W. He, Y. Li, H. Fan. J. Mater. Chem. **3**, 8852–8864 (2015).
[7] W.S. Woo, S.S. Won, C.W. Ahn, S.A. Chae, A. Ullah, W. Kim. J. Appl. Phys. **115**, 034107 (2014).
[8] T. Li, X.L. Li, Z.H. Zhao, H.M. Ji, Y. Dai. J. Integr. Ferroelectr. **162**, 1–7 (2015).
[9] S.V. Zubkov, I.A. Parinov, A.V. Nazarenko, Y.A. Kuprina. Springer Proceedings in Materials. **20**, 163–174 (2023).
[10] S. Dubey, O. Subohi, R. Kurchanic. Appl. Phys. A **124**, 461 (2018).
[11] S.V. Zubkov. Journal of Advanced Dielectrics **11**, 2160016 (2021).
[12] S.V. Zubkov, V.G. Vlasenko. Phys. Solid State **59**, 2303–2307 (2017).
[13] Y. Li, C.J. Lu, J. Su, C. Zhang, S.F. Zhao, X.X. Wang, D.J. Zhang, H.M. Yin. J. Alloys Compd. **687**, 707–711 (2016).
[14] J. Su, Y.Z. Long, Q. Li, C. Lu, K. Liang, J. Li, L. Luo, L. Sun, X. Lu, J. Zhu. J. Alloys Compd. **747**, 1002–1007 (2018).
[15] D.L. Zhang, L. Feng, W.C. Huang, W. Zhao, X. Li. J. Appl. Phys. **120**, 154105 (2016).
[16] F. Rehman, L. Wang, H.B. Jin, P. Ahmad, Y. Zhao, J.B. Li. Journal of Alloys and Compounds **709**, 686–691 (2017).
[17] V. Koval, I. Skorvanek, G. Viola, M. Zhang, C. Jia, H. Yan. J. Phys. Chem. C. **122**, *27*, 15733–15743 (2018).
[18] P.Y. Fang, L. Peng, Z.Z. Xi, W. Long, X. Li. J. Mater. Sci. Eng. B. **186**, 21–25 (2014).
[19] A. Faraz, J. Ricote, R. Jimenez, T. Maity, M. Schmidt, N. Deepak, S. Roy, M.E. Pemble, L. Keeney. J. Appl. Phys. **123**, 124101 (2018).
[20] Y.D. Qiu, S.F. Zhao, Z.P. Wang. Mater. Lett. **170**, 89–92 (2016).
[21] Y.L. Bai, J.Y. Chen, S.F. Zhao. RSC Adv. **6**, 41385–41391 (2016).
[22] D.F. Peng, H. Zou, C.N. Xu, X.S. Wang, X. Yao, J. Lin, T.T. Sun. AIP Adv. **2**, 042187 (2012).
[23] Z. Zhu, X.N. Li, W. Gu, J.L. Wang, H.L. Huang, R.R. Peng, X.F. Zhai, Z.P. Fu, Y.L. Lu. J. Alloys Compd. **686**, 306–311 (2016).
[24] Y. Li, M.Y. Bian, N.N. Zhang, W. Bai, J. Yang, Y. Zhang, X. Chu. Tang. J. Ceram. Int. **45**, 8634–8639 (2019).
[25] H. Sun, T. Yao, X. Xie, Y. Lu, Y. Wang, Z. Xu, J. Han, Chen, X.B. Ni. J. Colloid. Interf. Sci. **534**, 499–508 (2019).
[26] Y.H. Shu, Q.Q. Ma, L. Cao, Z. Ding, X. Chen, F. Yang. J. Alloys Compd. **773**, 934–939 (2019).
[27] H.Y. Zhao, H. Wang, Z.X. Cheng, Q.M. Fu, H. Tao, Z.B. Ma, T.T. Jia, H. Kimura, H.D. Li. Ceram. Int. **44**, 13226–13231 (2018).
[28] Y. Huang, L. Mi, J. Qin, S. Bi, H.J. Seo. J. Am. Ceram. Soc. **102**, 3555–3566 (2019).
[29] X.Z. Zuo, J. Yang, B. Yuan, D.P. Song, X.W. Tang, K.J. Zhang, X.B. Zhu, W.H. Song, J.M. Dai, Y.P. Sun. J. Appl. Phys. **117**, 114101 (2015).
[30] F. Rehman, L. Wang, H.B. Jin, A. Bukhtiar, R.B. Zhang, Y.J. Zhao, J.B. Li. J. Am. Ceram. Soc. **100**, 602–611 (2017).
[31] H. Zou, L. Jun, X.S. Wang, D.F. Peng, Y.X. Li, X. Yao. Opt. Mater. Exp. **4**, 1545–1554 (2014).
[32] C.A.-Pazde Araujo, J.D. Cuchiaro, L.D. McMillan, M.C. Scott, J.F. Scott. Nature London **374**, 627 (1995).
[33] T. Kikuchi. J. Alloys Compd. **48**, 319 (1976).
[34] Rajveer Singh, Vandna Luthra, R.S. Rawat, R.P. Tandona. Ceramics International **l41**, 4468–4478 (2015).
[35] Ismunandar, J.K. Brendan. J. Mater. Chem. 541–544 (2006).
[36] B.J. Kalaiselvi, R. Sridarane, Ramaswamy Murugana. Materials Science and Engineering **127**, 224–227 (2006).
[37] P. Banerjee, A. Franco. J. Materials Chemistry and Physics **225**, 213–218 (2019).
[38] Y. Wu, M.J. Forbess, S. Seraji, S.J. Limmer, T.P. Chou, C. Nguyen, G. Cao. J. Appl. Phys. **90**, 5296–5302 (2001).
[39] T. Wei, C.Z. Zhaonad, Q.J. Zhou, Z.P. Li, Y.Q. Wang, L.S. Zhang. Opt. Mater. **36**, *7*, 1209–1212 (2014).
[40] Maya Verma, Tanwar Amit, K. Mater. Chem. Phys. **209**, 159–164 (2018).
[41] Vaibhav Shrivastava. Ceram. Int. **42**, *8*, 10122–10126 (2016).
[42] M. Nagata, D.P. Vijay, X. Zhang, S.B. Desu. Phys. Status Solidi A, **157**, 75–82 (1996).
[43] P. Banerjee, A. Franco. J. Phys. Status Solidi **214**, *10*, 1700067 (2017).
[44] Y. Shimakawa, Y. Kubo, Y. Tauchi, T. Kamiyama, H. Asano, F. Izumi. Appl. Phys. Lett. **77**, 2749–51 (2000).
[45] S.M. Huang, Y.C. Li, C.D. Feng, M. Gu, X.L. Liu. J. Am. Ceram. Soc. **91**, 29332008 (2016).
[46] Y. Wu, M.J. Forbess, S. Seraji, S.J. Limmer, T.P. Chou, C. Nguyen, G. Cao. J. Appl. Phys. **90**, 5296 (2001).
[47] P. Fang, H. Fan, J. Li, F. Liang. J. Appl. Phys. **107**, 064104 (2010).
[48] S.M. Huang, C.D. Feng, L.D. Chen, X.W. Wen. Solid State Commun. **133**, 375 (2005).
[49] M. Verma, K. Sreenivas, V. Gupta. J. Appl. Phys. **105**, 024511 (2009).
[50] L. Sun, C.D. Feng, L.D. Chen, S.M. Huang. J. Appl. Phys. **101**, 084102 (2007).
[51] A. Speghini, M. Bettinelli, U. Caldiõ, M.O. Ramírez, D. Jaque, L.E. Bausá, J.G. Solé. J. Phys. D: Appl. Phys. **39**, 4930 (2006).

[52] Mohamed Afqir, Amina Tachafine, Didier Fasquelle, Mohamed Elaatmani, Jean Claude Carru, Abdelouahad Zegzouti, Mohamed Daoud. Applied Physics A. **124**, 83 (2018).
[53] S.V. Zubkov, I.A. Parinov, A.V. Nazarenko, A.V. Pavlenko. FTT **65**, *8*, 1297–1306 (2023). (in Russian).
[54] S.V. Zubkov, I.A. Parinov, A.V. Nazarenko, Yu.A. Kuprina. FTT **64**, *10*, 1475–1482 (2022). (in Russian).
[55] S.V. Zubkov, Y.A. Kuprina, I.A. Parinov. Electronics **11**, 2 (2022).
[56] S.V. Zubkov. Journal of Advanced Dielectrics **11**, *5*, 2160018 (2021).
[57] W. Kraus, G. Nolze. Powder Cell for Windows, Version2.3. Fed. Inst. Mater. Res. Test., Berlin (1999).
[58] S.N. Galii, M.B. Kopelevich, V.A. Khrenkin. Stend dlya issledovaniya kharakteristik p'ezomaterialov v sil'nykh elektricheskih polyakh „Petlya", Inzhenernyi vestnik Dona **3**, (2010). (in Russian).
[59] X.F. Du, I.W. Chen. J. Am. Ceram. Soc. **81**, 3253–9 (1998).
[60] V.A. Isupov. Ferroelectrics **189**, 211 (1996).
[61] V.A. Isupov. Neorgan. Materialy **421**, 353 (2006). (in Russian).
[62] Rajveer Singh, Vandna Luthra, R.S. Rawat, R.P. Tandona. Ceramics International **141**, 4468–4478 (2015).
[63] V.M. Goldschmidt. Geochemische Verteilungsgesetze der Elemente, J. Dybwad, Oslo, 1923 (1927).
[64] R.D. Shannon. Acta Crystallogr. A **32**, 751 (1976).
[65] B.J. Kennedy, B.A. Hunter. Chem. Mater. **13**, 4612 (2001).
[66] Y. Shimakawa, Y. Kubo. Appl. Phys. Lett. **74**, 290 (1999).
[67] N.C. Hyatt, J.A. Hriljac, T.P. Comyn. Mater. Res. Bull. **38**, 837 (2003).

Translated by M.Shevelev